Journal of Power Sources 250 (2014) 204–211

Contents lists available at ScienceDirect

Journal of Power Sources

journal homepage: www.elsevier.com/locate/jpowsour

Characterisation of a hybrid, fuel-cell-based propulsion system for small unmanned aircraft

D. Verstraete [a,*], K. Lehmkuehler [a], A. Gong [a], J.R. Harvey [b], G. Brian [b], J.L. Palmer [b]

[a] School of Aerospace, Mechanical and Mechatronic Engineering, The University of Sydney, Sydney, NSW 2006, Australia
[b] Aerospace Division, Defence Science and Technology Organisation, 506 Lorimer Street, Fishermans Bend, VIC 3207, Australia

HIGHLIGHTS

- An experimental characterisation is presented for the hybrid AeroStack fuel-cell system.
- The electrical efficiency of the fuel cell was found to be over 50% for a large range of output power.
- The polarisation curve exhibits hysteresis effect during dynamic load changes.
- The systems' battery ensures a fast response and protects the fuel cell from starvation.
- The fuel cell recharges the battery with a peak current of 1 A.

ARTICLE INFO

Article history:
Received 28 September 2013
Received in revised form
9 November 2013
Accepted 11 November 2013
Available online 19 November 2013

Keywords:
Characterisation
Hybrid fuel-cell-based system
Unmanned aircraft systems
Polarisation curve
Dynamic response

ABSTRACT

Advanced hybrid powerplants combining a fuel cell and battery can enable significantly higher endurance for small, electrically powered unmanned aircraft systems, compared with batteries alone. However, detailed investigations of the static and dynamic performance of such systems are required to address integration challenges. This article describes a series of tests used to characterise the Horizon Energy Systems' AeroStack hybrid, fuel-cell-based powertrain. The results demonstrate that a significant difference can exist between the dynamic performance of the fuel-cell system and its static polarisation curve, confirming the need for detailed measurements. The results also confirm that the AeroStack's lithium-polymer battery plays a crucial role in its response to dynamic load changes and protects the fuel cell from membrane dehydration and fuel starvation. At low static loads, the AeroStack fuel cell recharges the battery with currents up to 1 A, which leads to further differences with the polarisation curve.

1. Introduction

Small, electrically powered unmanned aircraft systems (UAS) are currently used for a variety of reconnaissance and remote-sensing missions [1–3]. Electric propulsion is typically preferred over the use of small internal-combustion engines because of its comparatively high efficiency, low cost, and high reliability [1,2,4–6], as well as low infrared and noise levels. The energy density of commercially available batteries, however, limits the achievable endurance of battery-powered UAS; and this has motivated the development of advanced fuel-cell-based powerplant systems [2,6–8]. Several research groups around the world have designed and flight-tested fuel-cell-powered demonstrator aircraft [2,4–16]. Their research systematically reports the lack of publicly available detailed performance specifications [6–8] and demonstrates that airworthy fuel-cell-based systems require a different design strategy than automotive and stationary applications [4,17].

Aircraft typically require a large power range for different flight phases, and a fast response is required to balance the load variations [6]. However, fuel cells are generally limited in power density and can suffer from a slow dynamic response [18–24]. A hybrid system, in which a fuel cell is combined with a secondary, short-term boost capacity, such as that provided by batteries or ultra-capacitors, is thus required for operationally viable systems [6,15]. These hybrid systems combine the high power density of the secondary system, ideal for short-duration peak power, with the high energy density of the fuel cell, which enables long endurance [19–21,24–28]. In a hybrid system, the advantages of each of the subsystems are exploited, which can lead to a lighter, cheaper system with improved efficiency [25–27]. Hybrid systems, however, include dynamic subsystems and passive or active power-

* Corresponding author.
E-mail address: Dries.Verstraete@sydney.edu.au (D. Verstraete).

0378-7753/$ – see front matter
http://dx.doi.org/10.1016/j.jpowsour.2013.11.017

Nomenclature

Δg_f	Gibbs free enthalpy of formation, [J mol^{-1}]
$\dot{m}_{H_2,tot}$	total H_2 mass-flow rate, [slpm]
$\dot{m}_{H_2}$	H_2 mass-flow rate (no purging), [slpm]
$\dot{n}_{H_2}$	H_2 molar-flow rate (no purging), [mol s^{-1}]
η_{el}	electrical efficiency, [−]
η_F	Faradic efficiency, [−]
η_{th}	thermodynamic efficiency, [−]
η_V	voltage efficiency, [−]
μ_f	fuel utilisation, [−]
a	number of stack cells, [−]
B	polarisation curve-fit coefficient, [V ln(A)$^{-1}$]
F	Faraday constant, [C mol^{-1}]
I	fuel-cell stack current, [A]
LHV	lower heating value of H_2, [MJ kg^{-1}]
lhv	molar lower heating value of H_2, [J mol^{-1}]
m	polarisation curve-fit coefficient, [V]
n	polarisation curve-fit coefficient, [A^{-1}]
P	fuel-cell stack power, [W]
V_0	polarisation curve-fit coefficient, [V]
R	polarisation curve-fit coefficient, [Ω]
V	fuel-cell stack voltage, [V]
A/D	analog-to-digital
d.c.	direct current
FS	full scale
LiPo	lithium-polymer
PEM	proton exchange membrane
UAS	unmanned aircraft systems

management systems, which present implementation challenges requiring proper consideration when integrating the powerplant in an (unmanned) aircraft.

Despite the documented need for detailed performance data and a hybrid architecture, most reports in the literature focus on the aircraft development and only present limited flight-test results on the performance of the propulsion system. Detailed investigations of the static and dynamic behaviour of fuel-cell power sources in UAS configurations are limited [5], and the performance of hybrid battery-fuel-cell systems for UAS is only superficially documented [6,15].

This paper describes a detailed characterisation of the Horizon Energy Systems' AeroStack[1] hybrid, fuel-cell-based powertrain, which is designed for use in small UAS [29,30]. Section 2 of the paper describes the architecture of the test bench, which has been arranged to permit future hardware-in-the-loop simulation. Section 3 presents the (static) polarisation curve of the hybrid system; and its dynamic response is described in Section 4.

2. Test-bench architecture

A schematic representation of the test bench used to characterise the hybrid system is given in Fig. 1. The hardware components tested in the current configuration are shown in the light-grey area of the figure. They consist of the AeroStack hybrid system, which comprises a fuel cell, its controller, a 6S-cell lithium-polymer (LiPo) battery, and a passive power-management board [29,30]. As illustrated in Fig. 1, the AeroStack fuel cell is supplied with high-purity (99.999%) hydrogen from pressurised bottles; and a load is applied using a direct-current (d.c.) electronic load.

2.1. Hardware components

The test bench is currently built around a hybrid AeroStack system from Horizon Energy Systems [29,30]. It includes a 35-cell proton exchange membrane (PEM) fuel-cell stack with an active area of 16.8 cm^2. The stack has a nominal power output of 200 W and can deliver up to 10 A [29,30]. Its operating voltage ranges from 32 V when no load is applied to 20 V at full load [29,30]. The fuel cell is self-humidified and operates at near-ambient cathode pressure. The anode (hydrogen side) is dead-ended so that all of the hydrogen is either consumed by the fuel-cell reaction or wasted due to leakage or purging.

The fuel-cell controller adjusts the stack temperature by controlling the speed of the cathode-supply fans, as indicated in Fig. 1. The controller also regulates periodic anode purging to maintain a high rate of hydrogen utilisation and to ensure stable, prolonged stack performance [30]. Anode purging is required to remove inert gases, liquid water and contaminants, as well as any excess hydrogen from the fuel-cell anode and to maintain internal pressure at appropriate levels [5,21,31–35]. Finally, the controller short-circuits the fuel cell every 10 s. This increases the stack efficiency and forms part of the self-humidification process of the fuel cell [36]. Short-circuiting is executed through a solid-state switch on the controller that is connected across the fuel cell's output terminals [36]. During short-circuiting, the load is disconnected from the fuel cell for about 50 ms, and the fuel cell does not supply power to either the load or its own controller [36]. The LiPo battery is included in the circuit to provide continuous power to the load and controller and to prevent total loss of power to either. The fuel-cell controller has a capacitor to smooth the power output, but its capacity is not sufficient to bridge the 50-ms gap completely [36].

Besides bridging the short-circuiting period, the 6S-cell ThunderPower 1350-mAh (25C) LiPo battery pack can deliver an additional 400 W for 2 min to meet the high-power requirements during UAS take-off or climbing [30]. The battery augments the power output from the fuel cell through the power-management board, and the total output power is limited to 800 W for approximately 1 min to prevent its Schottky diode from overheating [30]. The board additionally controls the recharging of the battery when excess power is available from the fuel cell.

2.2. Interface components

In the experimental arrangement described here, the interface components provide the physical and communication link between the software and the previously described hardware components. The electrical connection between the hybrid AeroStack system and the control software is made by use of a BK Precision 8514 d.c. electronic load [37]. This programmable multi-mode load can draw up to 1200 W and is rated up to 120 V and 240 A. In constant-power mode, the load has an accuracy of 1.0% ± 0.1% of the full scale (FS) [37].

As the AeroStack system does not provide a measurement of the hydrogen flow rate, a mass-flow meter is included on the test bench, so that the efficiency of the fuel cell can be determined. An Apex AX-M4SLPM-D5 flow meter has been selected because it offers a high repeatability (0.2% FS), coupled with a very high

[1] Horizon Energy Systems has recently rebranded its products, adopting the name AeroStack for the fuel-cell hybrid system and using AeroPak for the system including a chemical-hydride tank. To reflect this, the name AeroStack is used here.

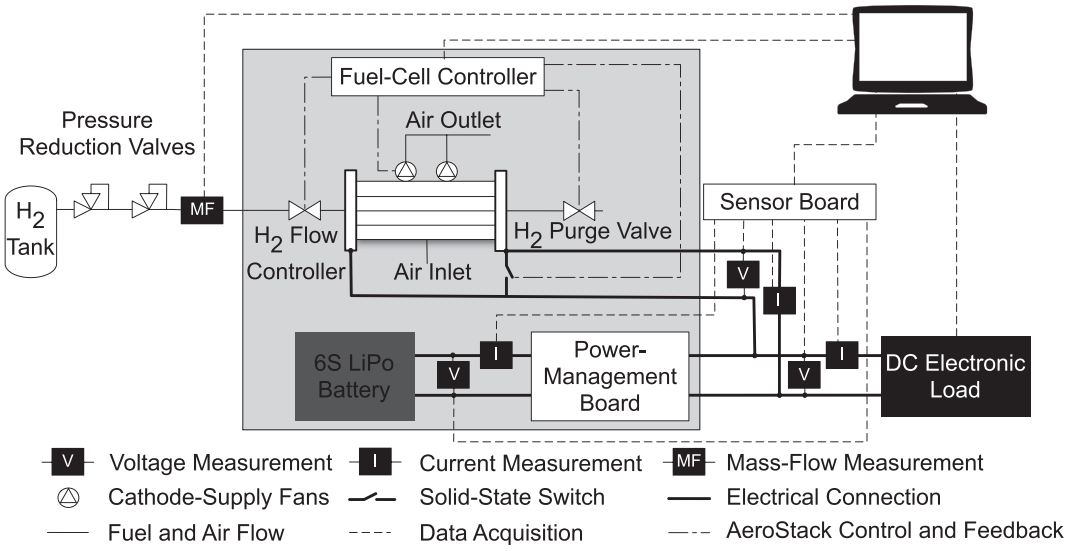

Fig. 1. Schematic of the test bench.

accuracy (0.2% of the reading), when custom calibrated [38]. As shown in Fig. 1, additional current and voltage measurements are made to verify the values reported by the AeroStack system. Eagle Tree Systems Hall-effect sensors are used for the current measurements. They measure 0–100 A in 50-mA increments and are calibrated before use with the BK Precision electronic load and an ET System LAB/SMS 435 d.c. power source. The fuel-cell and battery voltages are measured using voltage dividers consisting of two resistors in series to bring the voltage down to the 0–5 V range of the analog-to-digital (A/D) converters. The current and voltage measurements are recorded by use of an Arduino Pro Mini sensor board equipped with an 8-channel, 16-bit A/D converter from Linear Technologies (LTC1859). For the tests reported here, the outputs from the mass-flow meter and sensor board are sampled at 50 Hz to permit the capture of at least two samples during each short-circuiting period of the system. The d.c. electronic load is controlled at 2 Hz; and the AeroStack system reports the voltages of the fuel cell and battery, as well as the fuel-cell current, power, and temperature, at 1 Hz. The control of the electronic load and the data acquisition are performed using a Matlab® interface developed for the purpose.

3. AeroStack polarisation curve

The performance of fuel cells is typically presented in the form of a polarisation curve, which indicates the relationship between the fuel-cell stack voltage, V, and the stack current, I [5,39]. The polarisation curve indicates the static performance of the fuel-cell stack. As the fuel cell's control system regulates the temperature and evaporative cooling of the stack through the speed of the cathode-supply fans, the polarisation curve is influenced by the control system. This connection between the air-supply, water-management, and cooling systems leads to a nonlinear relationship amongst the cathode stoichiometry, membrane humidification, and stack temperature [5], which is represented by the polarisation curve.

The polarisation curve of the AeroStack PEM fuel cell is determined by measuring the stack current and voltage at its output. The measurements are made with the hybrid system delivering power in the range of 0–600 W and with the fuel cell operating under its normal thermal and stoichiometric control. For power settings below 300 W, each setting is maintained for ~100 s; whereas for higher power settings, this time is reduced linearly to ~30 s at 600 W to avoid excessively draining the LiPo battery. An inordinate depletion rate of the battery would lead to fluctuations in the system voltage during the testing period, which would change the recorded operating point. Reducing the testing time with increasing power minimises this effect.

The polarisation curve is represented in Fig. 2(a). Results from two measurements of the time–averaged voltage and current delivered by the fuel cell at each test point are depicted. A small difference can be seen between the voltage reported by the AeroStack and that obtained from the Arduino sensor board, particularly at low currents. The power level reported by the AeroStack system and that computed from the sensor-board measurements ($P = I \cdot V$) are, however, in very good agreement, as shown in Fig. 2(b).

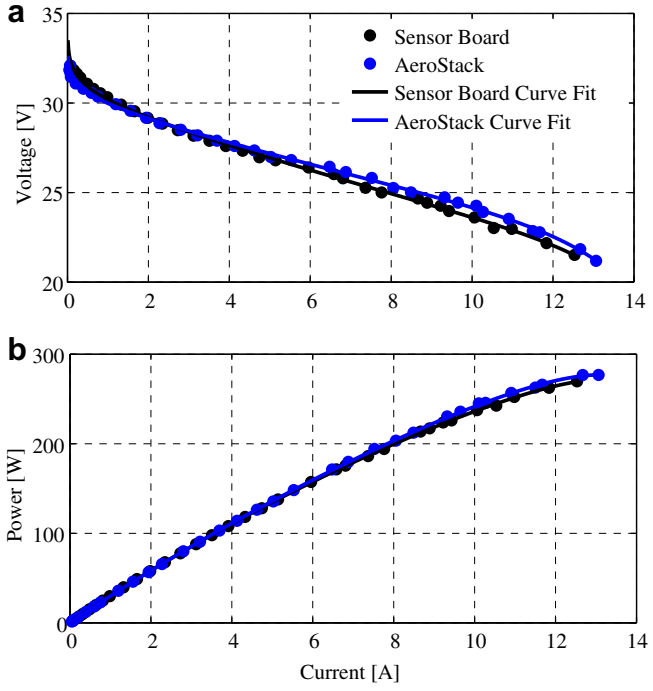

Fig. 2. (a) Fuel-cell polarisation curve and (b) output power vs. current.

Results from a curve fit of each dataset are also shown in Fig. 2(a). The curve fits are obtained with the following expression (adopted from Refs. [19,40–42]):

$$V = V_0 - B\cdot\ln(I) - R\cdot I - m\cdot\exp(n\cdot I), \quad (1)$$

and the coefficients of each curve fit and their coefficients of determination (R^2-values) are reported in Table 1. The coefficients are used to compute the polarisation and power–current curves shown in Fig. 2(b).

The activation-voltage drop due to the double layer of charge at the interfaces between the membrane and the electrodes [42–45] as well as to fuel-crossover and internal currents [45] is clearly noticeable in the region of small currents in Fig. 2(a). The activation-voltage drop is modelled by the logarithmic term in Eq. (1). At higher currents, the voltage depends linearly on the current, as shown by the $R\cdot I$ term in Eq. (1). This indicates the prevalence of Ohmic losses, caused by membrane resistance to the transfer of protons and electrical resistance of the electrodes [19,32,33,40,44,46]. At even higher currents, concentration (or diffusion) losses occur, as mass transfer limits the stack performance and results in a rapid voltage drop-off [19,42,46]. As indicated by the low value of the coefficient of the exponential term in Eq. (1) (m), this region cannot be reached with the AeroStack, as the controller prevents the fuel cell from operating at sufficiently high currents.

The measured rate at which fuel is consumed by the system, $\dot{m}_{H_2,tot}$ (which includes purged hydrogen) is shown in Fig. 3. The stack power is computed from the data in Fig. 2. Also shown is the fuel utilisation, which is defined as [47,48]:

$$\mu_f = \frac{\dot{m}_{H_2}}{\dot{m}_{H_2,tot}}, \quad (2)$$

where $\dot{m}_{H_2}$ is the hydrogen flow rate without the purged hydrogen (i.e., only the hydrogen that is reacted in the stack or steadily lost to leakage). The flow rate of hydrogen without purging is determined from the mass-flow-rate measurements by taking a moving average over a sample range of 10% of the total number of measurements for each operating point. Thus, the peaks in fuel-flow rate due to purging are filtered and smoothed; and a good approximation of the fuel utilisation is obtained without measuring the small, highly variable purging flow rate.

The total fuel consumption is roughly linear with the output power of the fuel cell, as shown on Fig. 3(a). A fuel utilisation of over 90% is obtained above 50 W (Fig. 3(b)). The utilisation drops to just above 40% at low power. This is consistent with other reports [7,8,32], which give peak utilisation values of 90–95%. The estimates of fuel utilisation above 140 W are slightly less accurate, as the mass-flow meter reaches its maximum capacity of 4.5 slpm during purging at those power levels.

The electrical efficiency computed from the two independent datasets represented in Fig. 2 is given in Fig. 4(a). The electrical efficiency, η_{el}, is defined as the ratio of the power output by the stack to that input to the system in the form of hydrogen [47,48]:

Table 1
Coefficients for curve fits shown in Fig. 2.

	AeroStack data	Sensor-board data
V_0 [V]	30.48	30.76
B [V ln(A)$^{-1}$]	0.4947	0.6281
R [Ω]	0.5002	0.5627
m [V]	$1.972\cdot10^{-4}$	$2.174\cdot10^{-5}$
n [A^{-1}]	0.6826	0.8192
R^2-value	0.9986	0.9987

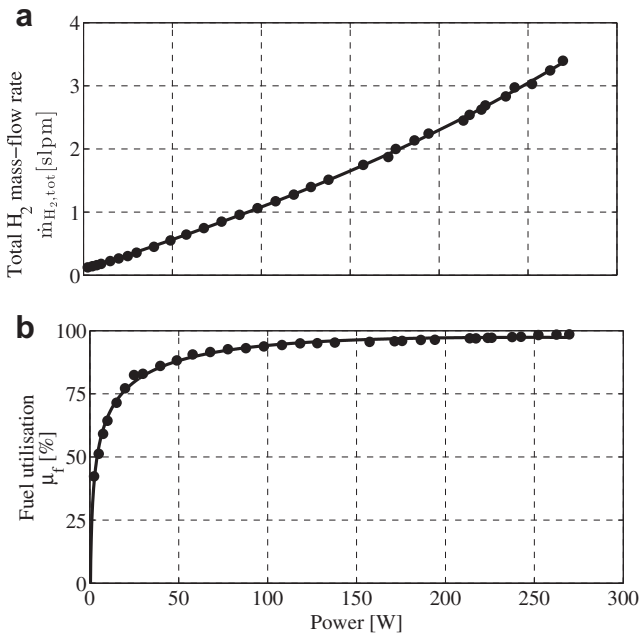

Fig. 3. (a) Total fuel consumption and (b) fuel utilisation as functions of fuel-cell output power.

$$\eta_{el} = \frac{I\cdot V}{\dot{m}_{H_2}\cdot LHV}, \quad (3)$$

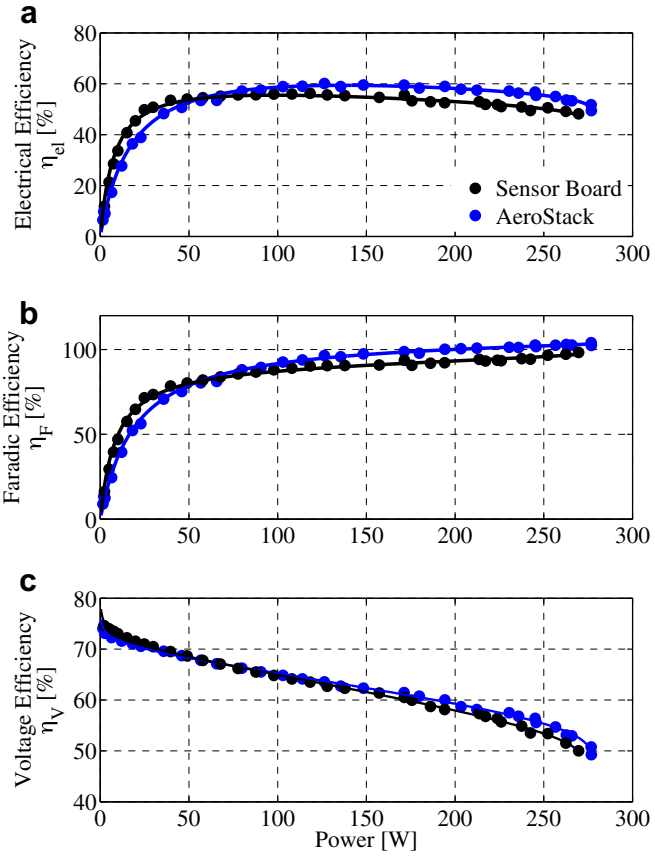

Fig. 4. (a) Electrical, (b) Faradic, and (c) voltage efficiencies as functions of fuel-cell output power.

where LHV is the lower heating value of hydrogen (120 MJ kg^{-1}). To assist with identifying the sources of "inefficiency", Fig. 4 also includes the Faradic and voltage efficiencies. The electrical efficiency can be decomposed as follows [47,48]:

$$\eta_{el} = \eta_{th} \cdot \eta_F \cdot \eta_V \cdot \mu_f, \quad (4)$$

where η_{th} is the thermodynamic or theoretical efficiency, η_F is the Faradic (or current) efficiency, and η_V is the voltage efficiency. The thermodynamic efficiency is defined as the ratio of the Gibbs free enthalpy of formation, Δg_f, to the fuel's molar lower heating value, lhv [42,47,48]:

$$\eta_{th} = \frac{\Delta g_f}{lhv}, \quad (5)$$

which yields a value of 98.1% for hydrogen. The Faradic efficiency, η_F, is given by [47,48]:

$$\eta_F = \frac{a \cdot I}{2 \cdot F \cdot \dot{n}_{H_2}}, \quad (6)$$

where F is the Faraday constant ($9.648 \cdot 10^4$ C mol^{-1}), $\dot{n}_{H_2}$ is the molar flow rate of the hydrogen reacted in the stack (without the purged hydrogen), and a is the number of cells in the stack. The factor of two in the denominator represents the valency of the reaction (two electrons per hydrogen molecule). Finally, the voltage efficiency, η_V, is given by [47,48]:

$$\eta_V = \frac{2 \cdot F \cdot V}{a \cdot \Delta g_f}. \quad (7)$$

As before, the coefficient of two accompanying the Faraday constant represents the valency of the reaction.

Fig. 4 shows that the electrical efficiency is above 50% for a wide range of power output. As in Fig. 2, significant differences are observable between the values measured via the sensor board and the values reported by the AeroStack system. However, both measurements indicate that the electrical efficiency exceeds 50% between 50 and 200 W, the nominal operating range of the fuel cell [30]. Fig. 4(b) shows that the low electrical efficiency at low power settings results from a low Faradic efficiency. At high power, the voltage efficiency drops, as the fuel cell operates at lower voltage. The Faradic efficiency is close to 100%, with values exceeding 100% computed from the data reported by the AeroStack system.

4. Dynamic behaviour of the AeroStack system

The static polarisation curve, as shown in Fig. 2(a), is often used for design-phase system modelling of fuel-cell vehicles and can generally be obtained from fuel-cell manufacturers. Knowledge of the dynamic behaviour of the hybrid power system is, however, crucial for UAS applications, as a fast response to throttle changes is essential. Thus the dynamic response of the AeroStack system to rapid load changes is characterised by creating a dynamic polarisation curve.

4.1. Dynamic polarisation curve

As discussed previously, the polarisation curve represents the nonlinear relationship between cathode stoichiometry, membrane humidification, and stack temperature. When fed by dry gases, membrane humidification depends on the amount of water produced by the electrolysis reaction, which is a function of the load, and the operating temperature. The production and evaporation rates of the water are thus time and load dependent [40]. Furthermore, the fuel-cell temperature affects the activity of the catalyst on the anode and cathode, the humidification state of the membrane, the saturation of the gas dynamic layers, and gas diffusion through the membrane [33]. Both the humidification and temperature therefore influence the dynamic performance of the fuel cell. To assess this impact, the AeroStack system is subjected to more rapid positive and negative load changes than those used in evaluating the static polarisation curve described previously. The load is ramped up from 0 to 300 W and returned to 0 W using the same load changes as for the static polarisation curve. Two complete test sequences are executed, with constant-load intervals of 2 s and with intervals of 20 s. The resulting dynamic polarisation curves are given in Fig. 5.

The dynamic polarisation curves clearly show that a hysteresis effect is present at both time intervals. A similar phenomenon is observed in Refs. [40,49–51] and the bistable current–voltage characteristic is thought to be related to the impact of autocatalytical water production on membrane conductivity [40,50,51]. For sudden increases in load, the water content may be slow to reach equilibrium because the production rate is time dependent. As a consequence, the membrane does not have the required humidity for efficient proton conductivity [40]; and a lower voltage is observed at a given current compared with the value obtained for a decreasing load. In the latter case, the membrane already contains the required water from the previous higher-load operating interval. The appearance of the bistable current–voltage characteristics in self-humidified operation suggests that stoichiometry is not constant during rapid load changes [51].

This is confirmed by the increase in the magnitude of the hysteresis when faster load changes are commanded, as shown in Fig. 5. In addition, the curve obtained with 2-s intervals is more irregular than the 20-s-interval curve due to the purging and short-circuiting of the fuel cell. As both purging and short-circuiting occur every 10 s, each 20-s interval includes two purging and two short-circuiting events. This is not the case for the 2-s operating intervals.

4.2. System response to fast load changes

The dynamic polarisation curves shown in Fig. 5 are obtained by commanding only modest load changes; however, tests with rapid, large load changes are also conducted. The AeroStack hybrid system is subjected to the following load sequence with abrupt changes: 0 W – 400 W – 0 W – 200 W – 0 W – 100 W – 0 W – 50 W – 0 W. Each power setting is maintained for 60 s. The resulting system response is illustrated in Figs. 6–8. The power evolution during the test is given in Fig. 6, while the variations in current and voltage are

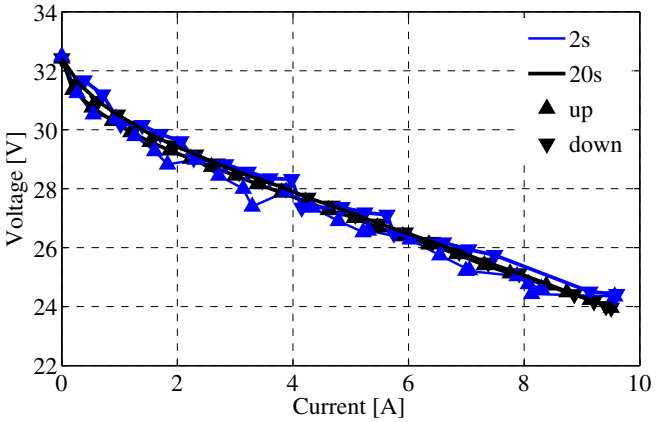

Fig. 5. Dynamic polarisation curves for test points at 2- and 20-s intervals.

shown in Figs. 7 and 8, respectively. The measurements obtained via the Arduino sensor board are filtered and smoothed using a moving average with a 1-s window to damp out fluctuations due to electromagnetic interference and the switching of the MOSFET on the power-management board. The smoothing does not obscure the effects of the short-circuiting, but does dampen the current and voltage fluctuations associated with those events.

The power delivered by the hybrid system accurately follows the commanded load changes, as can be seen in Fig. 6. When high power is suddenly requested, the battery ensures that the system responds rapidly, as shown by the first two power increases in Fig. 6. The battery provides a significant portion of the total power during the period when 400 W is demanded, but is active for only ~20 s following the step to 200 W, after which the fuel cell supplies the load. In contrast, for the 50- and 100-W steps, the battery does not supply power; and the entire load change is accommodated by the fuel cell. During these low-power periods, the fuel-cell stack is capable of meeting the change in load demand alone; and the battery output is cut off by the diode switch. An equivalent phenomenon was observed in Ref. [21].

The contribution of the battery to the larger load increases indicates that the fuel-cell controller limits the rate of increase of the current or power to prevent starvation due to a rapid drop in cell voltage. Rapid load changes can induce temporary membrane dehydration due to electro-osmotic drag on the anode side [21,52] and air-feeding starvation on the cathode side [21–24,53,54]. Starvation occurs when reactants are consumed faster than they can be supplied and can cause degeneration of the cells. To prevent oxidant starvation, the cathode mass flow needs to be adjusted rapidly. However, the inertia and the time lag in the control of the fans limit the rate at which the mass-flow rate can be increased. To reduce the risk of starvation, the dynamics of the load change can be constrained or a fast-responding auxiliary power source can be added [24,53,54].

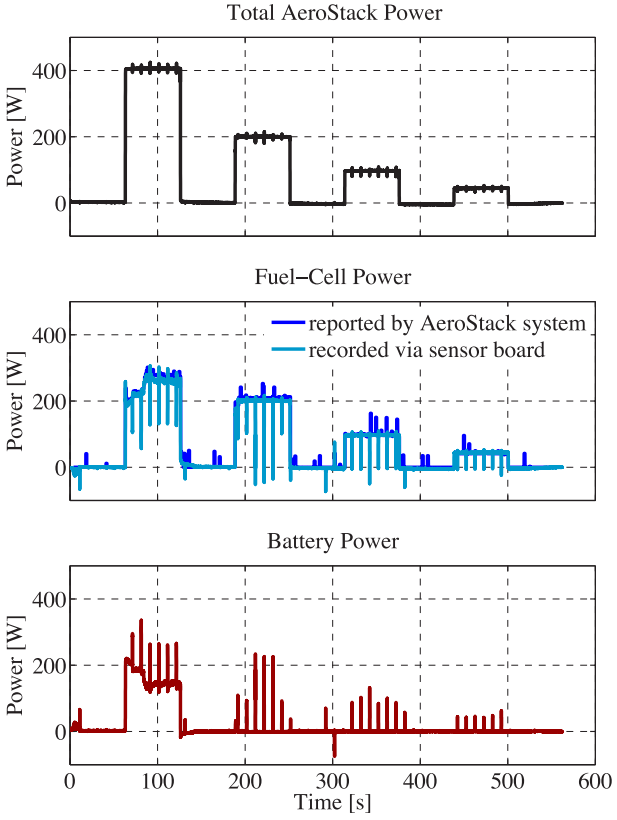

Fig. 6. Power evolution during the dynamic test.

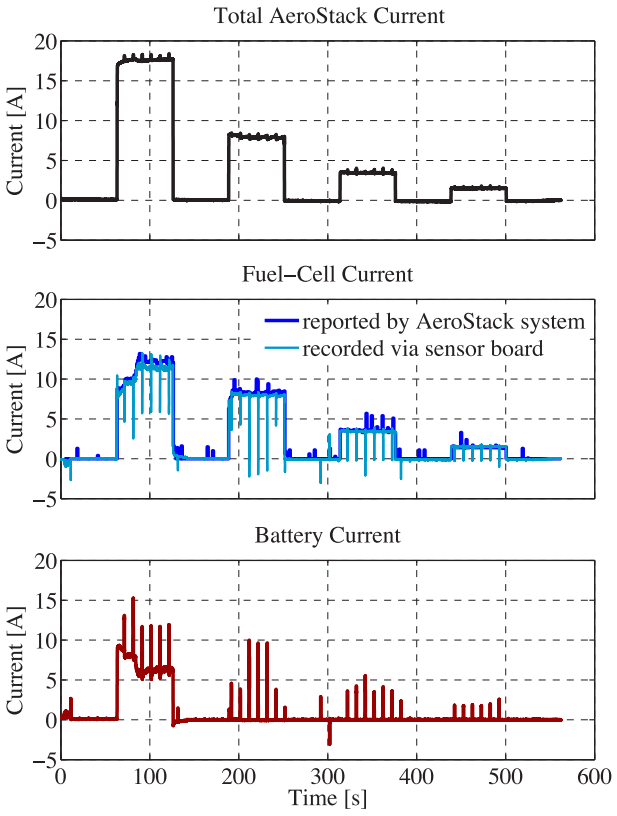

Fig. 7. Current evolution during the dynamic test.

The current and voltage histories, shown in Figs. 7 and 8, respectively, highlight the role of the power-management board of the AeroStack hybrid system. The fuel-cell voltage, as reported by the AeroStack system and as measured via the sensor board, follows the battery voltage closely when a high load is drawn (Fig. 8). The battery voltage reported by the AeroStack system is lower than the

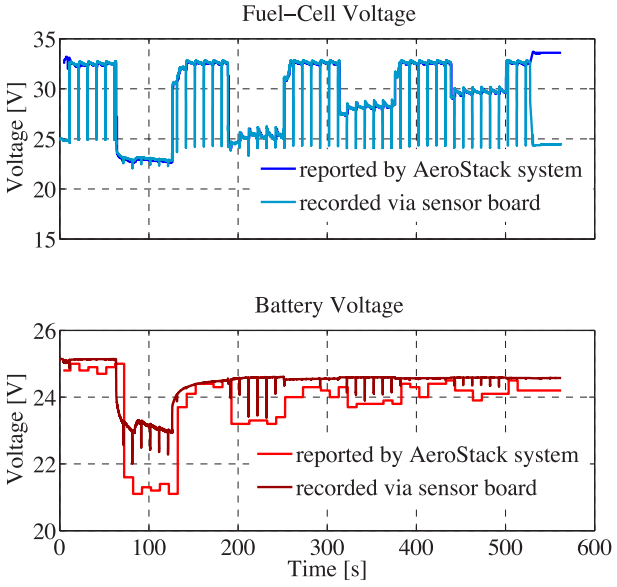

Fig. 8. Voltage evolution during the dynamic test.

running-average recorded via the sensor board, because the system reports the battery voltage only during periods of short-circuiting (when the entire load is drawn from the battery and its voltage drops temporarily). However, the battery-voltage values reported by the AeroStack system closely match the minimum values (troughs) in the raw data obtained via the sensor board (before temporal averaging).

The negative battery current around ~120 s on Fig. 7 shows that the battery is recharged by the fuel cell when the demanded power drops from 400 to 0 W. The fuel cell supplies a peak current of ~1 A to the battery. Whereas the current drops off rapidly, charging continues until the battery voltage reaches ~24.5 V. After the 200-W step, a similar phenomenon occurs, albeit at much lower currents.

The measured current levels, shown in Fig. 7 also indicate that higher current fluctuations occur at higher loads. This is because operation under higher-power conditions leads to an increase in fuel-cell temperature. The controller attempts to regulate the temperature by changing the speed of the fans, which causes both a higher power consumption by the fans and current fluctuations [55].

Furthermore, the fuel cell takes around 20 s to reach its peak output after a load change, as can be observed from the data in Fig. 6. This delay suggests that the transient response is limited by membrane hydration. As shown in Refs. [52,56], membrane dry-out due to electro-osmotic drag occurs relatively quickly, but it takes several seconds for water back-diffusion to re-wet the anode side. A time constant of ~10 s is given in Ref. [56] for this phenomenon, which is consistent with the observed transients in Figs. 6–8. During the high-load transients, a current overshoot and voltage undershoot are also observed. An equivalent phenomenon was observed in Refs. [21], where the effect was attributed to an integrative influence of both the charge double-layer effect and mass-transfer mechanisms. According to Ref. [21], the water and gas transport and distribution strongly influence the overshoot/undershoot behaviours in different current ranges; and large, rapid load changes could induce temporary dehydration.

5. Conclusion

Advanced fuel-cell-based hybrid powerplants can offer significant operational advantages for small unmanned aircraft systems over more traditional systems; however, a detailed understanding of the impact of their system dynamics is required for their integration into unmanned vehicles. The system dynamics associated with Horizon Energy Systems' AeroStack hybrid, fuel-cell-based powertrain are investigated. The results show that the dynamic performance of the system can differ significantly from its static performance, thereby confirming the need for such testing. The following conclusions can be drawn:

- The fuel-cell controller prevents the system from operating in the region of high concentration losses.
- The fuel utilisation of the AeroStack is above 90% from 50 W to 200 W, and an electrical efficiency of over 50% is obtained for this power range.
- The dynamic polarisation curve shows hysteresis due to water and temperature management.
- When the load is reduced, the AeroStack fuel cell recharges the depleted battery with currents of up to 1 A.

The results also demonstrate that the AeroStack system's LiPo battery plays a crucial role in the dynamic response of the system to rapid load changes and protects the fuel cell from membrane dehydration and fuel starvation. The battery provides a significant portion of the requested load at high power levels and when large load increases are demanded. However, for smaller load increases, the battery does not contribute, as it is isolated by a diode on the AeroStack's power-management board.

Acknowledgements

This work was partially funded by the Defence Science and Technology Organisation through its Strategic Research Initiative on Signatures, Materials, and Energy. Additional funding was obtained from the Early Career Researcher Program of the Faculty of Engineering & IT and the R.W. McKenzie Resource Center for Teaching and Research in Aeronautical Science and Technology at The University of Sydney. The authors would like to thank Joshua Barnes at The University of Sydney for his contributions to the design and construction of the test bench. Richard Liow, Li Aidan, Craig Knight, and Taras Wankewycz of Horizon Energy Systems are acknowledged for their support during this project.

References

[1] O. Gur, A. Rosen, J. Aircr. 46 (2009) 1340–1353.
[2] K. Kim, T. Kim, K. Lee, S. Kwon, J. Power Sources 196 (2011) 9069–9075.
[3] Y. Shin, S.-H. Chang, S.-O. Koo, Proc. Inst. Mech. Eng. Part D J. Automob. Eng. 219 (2005) 573–581.
[4] T.H. Bradley, B.A. Moffitt, T.F. Fuller, D.N. Mavris, D.E. Parekh, J. Aircr. 46 (2009a) 1945–1956.
[5] T.H. Bradley, B.A. Moffitt, D.N. Mavris, T.F. Fuller, D.E. Parekh, J. Propul. Power 25 (2009b) 1336–1344.
[6] T. Kim, S. Kwon, Int. J. Hydrogen Energy 37 (2012) 615–622.
[7] T.H. Bradley, B.A. Moffitt, D.N. Mavris, D.E. Parekh, J. Power Sources 171 (2007) 793–801.
[8] G. Rhoads, T. Bradley, N. Wagner, B. Taylor, D. Keen, in: 8th Annual International Energy Conversion Engineering Conference, American Institute of Aeronautics and Astronautics, Paper AIAA-2010-6690, 2010.
[9] C. Chiang, C. Herwerth, M. Mirmirani, A. Ko, S. Matsuyama, S.B. Choi, N. Nomnawee, D. Gamble, A. Arena, G. Gu, T. Wankewycz, A. Koschany, P. Jin, in: 46th AIAA Aerospace Sciences Meeting and Exhibit, American Institute of Aeronautics and Astronautics, Paper AIAA-2008-151, 2008.
[10] C. Herwerth, C. Chiang, A. Ko, S. Matsuyama, S.B. Choi, M. Mirmirani, D. Gamble, R. Paul, V. Sanchez, A. Arena, A. Koschany, G. Gu, T. Wankewycz, P. Jin, in: Aerospace Technology Conference and Exposition, 2007. SAE Technical Paper 2007-01-3930.
[11] B. Lee, P. Park, C. Kim, S. Yang, S. Ahn, J. Mech. Sci. Technol. 26 (2012) 2291–2299.
[12] U. Ofoma, C. Wu, in: AIAA 3rd "Unmanned Unlimited" Technical Conference, Workshop and Exhibit, Infotech Aerospace Conferences, American Institute of Aeronautics and Astronautics, Paper AIAA-2004-6384, 2004.
[13] R.O. Stroman, J.C. Kellogg, K. Swider-Lyons, in: 42nd Power Sources Conference, pp. 487–490.
[14] T.A. Ward, N. Jenal, ECS Trans. 26 (2010) 433–444.
[15] M. Dudek, P. Tomczyk, P. Wygonik, M. Korkosz, P. Bogusz, B. Lis, Int. J. Electrochem. Sci. 8 (2013) 8442–8463.
[16] D. Verstraete, J.R. Harvey, J.L. Palmer, in: 28th International Congress of the Aeronautical Sciences, 2012. Paper ICAS-2012-656.
[17] T. Bradley, B. Moffitt, T.F. Fuller, D. Mavris, D. Parekh, in: 26th AIAA Applied Aerodynamics Conference, American Institute of Aeronautics and Astronautics, Paper AIAA-2008-6413, 2008.
[18] Z. Jiang, L. Gao, M.J. Blackwelder, R.A. Dougal, J. Power Sources 130 (2004) 163–171.
[19] A. Jossen, J. Garche, H. Doering, M. Goetz, W. Knaupp, L. Joerissen, J. Power Sources 144 (2005) 395–401.
[20] C. Sapienza, L. Andaloro, F.V. Matera, G. Dispenza, P. Cret, M. Ferraro, V. Antonucci, Int. J. Hydrogen Energy 33 (2008) 3230–3234.
[21] Y. Tang, W. Yuan, M. Pan, Z. Wan, Appl. Energy 88 (2011) 68–76.
[22] P. Thounthong, V. Chunkag, P. Sethakul, S. Sikkabut, S. Pierfederici, B. Davat, J. Power Sources 196 (2011) 313–324.
[23] P. Thounthong, S. Raël, B. Davat, J. Power Sources 193 (2009) 376–385.
[24] T. Yalcinoz, M.S. Alam, Int. J. Hydrogen Energy 33 (2008) 1932–1940.
[25] R.K. Ahluwalia, X. Wang, J. Power Sources 139 (2005) 152–164.
[26] R.K. Ahluwalia, X. Wang, A. Rousseau, J. Power Sources 152 (2005) 233–244.
[27] Q. Cai, D.J.L. Brett, D. Browning, N.P. Brandon, J. Power Sources 195 (2010) 6559–6569.
[28] P. Corbo, F. Migliardini, O. Veneri, Int. J. Hydrogen Energy 34 (2009) 4635–4644.
[29] Horizon Energy Systems, Aeropak Brochure, vol. 2013, last accessed July 2013. http://www.hes.sg/files/AEROPAK.pdf.

[30] Horizon Energy Systems, Aeropak Technical Data Sheet, vol. 2013, last accessed July 2013. http://www.hes.sg/files/AEROPAK_Technical_Data_Sheet.pdf.
[31] F. Chen, Y.-G. Su, C.-Y. Soong, W.-M. Yan, H.-S. Chu, J. Electroanal. Chem. 566 (2004) 85–93.
[32] P. Corbo, F.E. Corcione, F. Migliardini, O. Veneri, Energy Convers. Manage. 47 (2006) 3255–3271.
[33] A.J. del Real, A. Arce, C. Bordons, J. Power Sources 173 (2007) 310–324.
[34] F. Philipps, G. Simons, K. Schiefer, J. Power Sources 154 (2006) 412–419.
[35] A. Sripakagorn, N. Limwuthigraijirat, Int. J. Hydrogen Energy 34 (2009) 6036–6044.
[36] Personal Communication, Horizon Energy Systems, 2013.
[37] BK Precision, User Manual 8500 Series DC Electronic Loads, last accessed July 2013. http://www.bkprecision.com/downloads/manuals/en/85xx_manual.pdf.
[38] Apex, Precision Gas Flow Meter Operating Manual, last accessed June 2013. http://www.apexvacuum.com/pdfs/ApexMassFlowMeterManual.pdf.
[39] C. Ziogou, S. Voutetakis, S. Papadopoulou, M.C. Georgiadis, Comput. Chem. Eng. 35 (2011) 1886–1900.
[40] J. Hamelin, K. Agbossou, A. Laperrière, F. Laurencelle, T.K. Bose, Int. J. Hydrogen Energy 26 (2001) 625–629.
[41] M.J. Kim, H. Peng, C.-C. Lin, E. Stamos, D. Tran, in: American Control Conference, 2005, pp. 3859–3864.
[42] J. Larminie, A. Dicks, Fuel Cell Systems Explained, second ed., Wiley, 2003.
[43] S. Lazarou, E. Pyrgioti, A.T. Alexandridis, J. Power Sources 190 (2009) 380–386.
[44] U. Reggiani, L. Sandrolini, G.L. Giuliattini Burbui, J. Power Sources 165 (2007) 224–231.
[45] A. Saadi, M. Becherif, A. Aboubou, M.Y. Ayad, Renew. Energy 56 (2013) 64–71.
[46] C.H. Zheng, Y.I. Park, W.S. Lim, S.W. Cha, Int. J. Automot. Technol. 13 (2012) 979–985.
[47] P. Corbo, F.E. Corcione, F. Migliardini, O. Veneri, J. Power Sources 157 (2006) 799–808.
[48] R. Neto, J. Teixeira, J. Azevedo, Int. J. Hydrogen Energy 38 (2013) 5348–5356.
[49] S. Bégot, F. Harel, J.M. Kauffmann, Fuel Cells 8 (2008) 23–32.
[50] H. Yu, C. Ziegler, J. Electrochem. Soc. 153 (3) (2006) A570–A575.
[51] R. Hanke-Rauschenbach, M. Mangold, K. Sundmacher, J. Electrochem. Soc. 155 (2) (2006) B97–B107.
[52] Y. Wang, C.-Y. Wang, Electrochim. Acta 51 (2006) 3924–3933.
[53] M.A. Danzer, S.J. Wittmann, E.P. Hofer, J. Power Sources 190 (2009) 86–91.
[54] A. Vahidi, A. Stefanopoulou, P. Huei, in: American Control Conference, vol. 1, 2004, pp. 834–839.
[55] V. Yufit, N.P. Brandon, J. Power Sources 196 (2011) 801–807.
[56] Y. Wang, C.-Y. Wang, Electrochim. Acta 50 (2005) 1307–1315.